Heavy Quark Vacuum Polarization Function at $\mathcal{O}(\alpha_s^2)$ and $\mathcal{O}(\alpha_s^3)$

André H. Hoang*,[1] Vicent Mateu†,[1] and S. Mohammad Zebarjad‡[1,2]

[1] *Max-Planck-Institut für Physik*
(Werner-Heisenberg-Institut)
Föhringer Ring 6, 80805 München, Germany

[2] *Physics Department, College of Sciences, Shiraz University*
Shiraz 71454, Iran

We determine the full mass and q^2 dependence of the heavy quark vacuum polarization function $\Pi(q^2)$ and its contribution to the total e^+e^- cross section at $\mathcal{O}(\alpha_s^2)$ and $\mathcal{O}(\alpha_s^3)$ in perturbative QCD. We use known results for the expansions of $\Pi(q^2)$ at high energies, in the threshold region and around $q^2 = 0$, conformal mapping and the Padé approximation method. From our results for $\Pi(q^2)$ we determine numerically at $\mathcal{O}(\alpha_s^3)$ the previously unknown non-logarithmic contributions in the high-energy expansion at order $(m^2/q^2)^i$ for $i = 0, 1$ and the coefficients in the expansion around $q^2 = 0$ at order q^{2n} with $n \geq 2$. We also determine at $\mathcal{O}(\alpha_s^2)$ the previously unknown $\mathcal{O}(v^0)$ constant term in the expansion of $\Pi(q^2)$ in the threshold region, where v is the quark velocity. Our method allows for a quantitative estimate of uncertainties and can be systematically improved once more information in the three kinematic regions becomes available by future multi-loop computations. For the contributions to the total e^+e^- cross section at $\mathcal{O}(\alpha_s^2)$ we confirm results obtained earlier by Chetyrkin, Kühn and Steinhauser.

MPP-2008-83
arXiv:0807.4173 [hep-ph]

* Electronic address: ahoang@mppmu.mpg.de
† Electronic address: mateu@mppmu.mpg.de
‡ Electronic address: zebarjad@susc.ac.ir

I. INTRODUCTION

The vacuum polarization function $\Pi(q^2)$ defined by the correlator of two electromagnetic currents $j^\mu(x) = \bar{\psi}(x)\gamma^\mu\psi(x)$,

$$\left(g_{\mu\nu}q^2 - q_\mu q_\nu\right)\,\Pi(q^2) \;=\; -\,i\int \mathrm{d}x\, e^{iqx}\,\langle\,0\,|T\,j_\mu(x)j_\nu(0)|\,0\,\rangle\;, \tag{1}$$

where q^μ is the four-momentum of the quark pair produced or annihilated by j^μ, represents an important quantity for theoretical studies as well as for many practical phenomenological applications. Relevant applications for the case of massive quarks include predictions of the hadronic cross section $R \sim \mathrm{Im}[\Pi]$, or sum rules for the determination of the heavy quark masses [1, 2]. These sum rules are based on moments of the cross section for heavy quark pair production

$$M_n \;=\int_{4m^2}^{\infty}\frac{\mathrm{d}s}{s^{n+1}}\,R(s)\,, \tag{2}$$

which in fixed-order perturbation theory are related to the expansion coefficients of $\Pi(q^2)$ around $q^2 = 0$,

$$\Pi(q^2\approx 0, m^2) \;=\; \frac{1}{12\,\pi^2\,Q_q^2}\sum_{n=1}^{\infty} M_n\,q^{2n}\,, \tag{3}$$

where Q_q is the heavy quark electric charge. In general the knowledge of the full dependence of the vacuum polarization function $\Pi(q^2)$ on q^2 and the quark mass m is desirable to avoid having to rely on approximations that are only valid in certain kinematic regimes.

At $\mathcal{O}(\alpha_s)$ the full mass and q^2 dependence of the vacuum polarization function is known from analytic computations carried out in Ref. [3]. At $\mathcal{O}(\alpha_s^2)$ analogous analytic results exist for the contributions that originate from inserting the massive [4, 5] and massless [6] fermion loops into $\mathcal{O}(\alpha_s)$ one-gluon exchange diagrams. For the other $\mathcal{O}(\alpha_s^2)$ contributions results for the expansions of $\Pi(q^2)$ in the high-energy limit, $|q^2| \to \infty$, the nonrelativistic threshold regime, $q^2 \approx 4m^2$, and in the Euclidean region around $q^2 = 0$ were used to reconstruct an accurate approximation [7, 8]. The method is based on the definition of subtraction functions which account for all logarithmic terms that arise for the expansions in the high-energy limit and in the threshold region. Using a conformal transformation to a new variable ω the full q^2 and mass dependence in the complex plane of the remaining contributions can be mapped into the unit circle rendering those contributions to an analytic function in the variable ω. The latter can then be successfully approximated by Padé approximants using the remaining expansion coefficients that are not related to logarithmic terms. With a large number of expansion coefficients for the three kinematic limits the full mass and q^2 dependence of the $\mathcal{O}(\alpha_s^2)$ vacuum polarization function can be determined with small numerical uncertainties.

For the $\mathcal{O}(\alpha_s^3)$ vacuum polarization there is also no fully analytic result available in the literature. A numerical study of the full $\mathcal{O}(\alpha_s^3 n_f^2)$ double fermionic contributions to the vacuum polarization function can be found in Ref. [9]. In the high-energy expansion its contributions to the total cross section up to order $(m^2/q^2)^2$ are known [10]. A comprehensive review of these results can be found in Ref. [11]. Moreover, in the threshold region, where an expansion in the small quark velocity v can be carried out, the $\mathcal{O}(\alpha_s^3)$ contributions to the total cross section at order $1/v^i$ for $i = 2, 1, 0$ are available from a factorization theorem for the heavy quark-antiquark pair production cross section in nonrelativistic QCD (NRQCD) at next-to-next-to-leading order (NNLO) [12, 13]. More recently also the moments M_1 [14, 15] and M_2 [16] at $\mathcal{O}(\alpha_s^3)$ have become available using elaborate high-power computer algebra tools.

In this work we use the presently available information on the $\mathcal{O}(\alpha_s^3)$ corrections to the vacuum polarization function $\Pi(q^2)$ in the high-energy limit, in the threshold region and the small q^2 domain to reconstruct the full q^2 and mass dependence of the vacuum polarization function at $\mathcal{O}(\alpha_s^3)$. The method we use is similar to the approach of Refs. [7, 8] employed previously for the $\mathcal{O}(\alpha_s^2)$ corrections of the vacuum polarization function (see also Refs. [17, 18, 19]), but also accommodates a few notable differences which are motivated by the fact that less information is known on the vacuum polarization function at $\mathcal{O}(\alpha_s^3)$. While in Refs. [7, 8] information from the high-energy expansion up to order (m^2/q^2) and from the threshold expansion up to next-to-leading order (NLO) was incorporated for the reconstruction, we account for the expansions up to order $(m^2/q^2)^2$ at high energies and up to NNLO in the threshold region. While in Ref. [7, 8] the full set of terms in the high-energy expansion of Π was used for the construction, in this work we only rely on the terms that carry an absorptive part and that contribute to the cross section above threshold. We show that our method allows to determine previously unknown non-logarithmic terms of the vacuum polarization at $\mathcal{O}(\alpha_s^3)$ in the high-energy expansion with very small errors. Moreover, while in Ref. [7, 8] and later in Ref. [20]

the coefficients of the small-q^2 expansion were included up to order q^{14} and q^{16}, respectively, we only rely on the presently available $\mathcal{O}(\alpha_s^3)$ coefficients up to order q^4. Our method allows to determine the expansion coefficients at order q^{2n} with $n \geq 3$. The results allow to compute the corresponding moments M_n in the fixed-order expansion at $\mathcal{O}(\alpha_s^3)$. For phenomenologically relevant values of n the error in the M_n due to the uncertainties in these coefficients is an order of magnitude smaller than the remaining scale-uncertainties of the M_n at $\mathcal{O}(\alpha_s^3)$. We demonstrate the reliability of the results by using the same approach for determining the corresponding coefficients for the vacuum polarization function at $\mathcal{O}(\alpha_s^2)$ where their values are well known analytically from the computations of Feynman diagrams. Another noteworthy difference of our approach to Refs. [7, 8] is that we implement a continuous set of subtraction functions to have a more reliable estimation of the uncertainty inherent to the method. Our approach can systematically incorporate new information from the expansions in the three kinematical regions, once it becomes available.

One important application of the vacuum polarization function at $\mathcal{O}(\alpha_s^3)$ obtained in this work is an analysis of low-n moments of the $e^+e^- \to c\bar{c}$ cross section to determine the $\overline{\rm MS}$ charm quark mass $\overline{m}_c$ and to investigate the uncertainty in $\overline{m}_c$ that arises from the difference of using fixed-order and contour-improved perturbation theory. For using contour-improved perturbation theory, which involves integrations of $\Pi(q^2)$ in the complex q^2-plane, it is essential to have the full mass and q^2 dependence of the vacuum polarization function. Such an analysis was carried out in Ref. [21] at $\mathcal{O}(\alpha_s^2)$. Determinations of the charm quark mass $\overline{m}_c$ using the vacuum polarization function at $\mathcal{O}(\alpha_s^3)$ in the fixed-order expansion alone were carried out recently in Refs. [15, 22]. In this paper we discuss in detail the reconstruction of the full q^2 and mass dependence of the $\mathcal{O}(\alpha_s^2)$ and $\mathcal{O}(\alpha_s^3)$ corrections to the vacuum polarization function as outlined above. The thorough analysis of uncertainties in the charm and bottom quark $\overline{\rm MS}$ masses obtained from low-n moments of the e^+e^- cross section will be given in a subsequent publication.

The program of this paper is as follows: In Sec. II we set up our notation and in Sec. III we present the basic features of our method for reconstructing the vacuum polarization function. In Sec. IV we explain details about how logarithmic contributions in the expansions in the threshold region and for high energies are incorporated and in Sec. V we present how the remaining non-logarithmic terms are treated. Some of the solutions we obtain have unphysical properties. Criteria that allow to identify and discard such solutions are discussed in Sec. VI. Numerical analyses for the $\mathcal{O}(\alpha_s^2)$ and $\mathcal{O}(\alpha_s^3)$ contributions of the vacuum polarization function are given in Secs. VII and VIII. Our conclusions are given in Sec. IX.

II. NOTATION

The relation between the normalized e^+e^- cross section R and and the vacuum polarization function Π reads

$$R(q^2) \,=\, 12\pi\, Q_q^2\, \mathrm{Im}\,\Pi(q^2 + i0, m^2)\,, \tag{4}$$

where Q_q is the heavy quark electric charge. The perturbative fixed-order expansion of $\Pi(q^2, m^2)$ has the form

$$\begin{aligned}\Pi(q^2, m^2) \,=\, \Pi^{(0)}(q^2, m^2) \,+\, \left(\frac{C_F\,\alpha_s(\mu^2)}{\pi}\right)\,\Pi^{(1)}(q^2, m^2) \\ +\, \left(\frac{\alpha_s(\mu^2)}{\pi}\right)^2\,\Pi^{(2)}(q^2, m^2, \mu^2) \,+\, \left(\frac{\alpha_s(\mu^2)}{\pi}\right)^3\,\Pi^{(3)}(q^2, m^2, \mu^2) \,+\, \cdots\,,\end{aligned} \tag{5}$$

with the color factor $C_F = 4/3$. We use the on-shell normalization of the vacuum polarization function, where

$$\Pi(0, m^2) \,=\, 0\,. \tag{6}$$

We exclude the so-called singlet contributions where the vacuum polarization function contains a three-gluon cut. Note that in this work we do not distinguish between the contributions in $\Pi^{(2)}$ and $\Pi^{(3)}$ proportional to the different SU(3) group theory color factors since there isn't any compelling technical reason that would make such a distinction mandatory. This approach neglects the existence of the multi-particle cuts from diagrams with the insertion of massive fermion loops. Their contribution is strongly phase-space-suppressed and can be safely ignored for the level of accuracy intended in this work. We emphasize, however, that our approach can be applied to the individual color contributions as well.

For the reconstruction of the vacuum polarization function accomplished in this work we use exclusively the pole mass scheme, $m = m_{\rm pole}$, since it allows for the most transparent treatment of the information from the quark pair

production threshold. Moreover we use the choice $\mu = m = m_{\rm pole}$ for the renormalization scale and generally suppress the μ-dependence of the functions $\Pi^{(i)}$. To simplify the presentation we frequently use the variable

$$z \equiv \frac{q^2}{4m^2}\,. \tag{7}$$

For the strong coupling we use $n_f = n_\ell + 1$ active running flavors, where quarks that are heavier than those produced by the current j^μ are integrated out and where all n_ℓ light flavors are treated as massless.

The analytic expression for the vacuum polarization functions at $\mathcal{O}(\alpha_s)$ [3] is an important ingredient of our analysis. The corresponding contributions using the notation of Eq. (5) have the form

$$\begin{aligned}
\Pi^{(0)} &= \frac{3}{16\pi^2}\left[\frac{20}{9} + \frac{4}{3z} - \frac{4(1-z)(1+2z)}{3z}G(z)\right],\\
\Pi^{(1)} &= \frac{3}{16\pi^2}\left[\frac{5}{6} + \frac{13}{6z} - \frac{(1-z)(3+2z)}{z}G(z) + \frac{(1-z)(1-16z)}{6z}G^2(z) - \frac{(1+2z)}{6z}\left(1+2z(1-z)\frac{d}{dz}\right)\frac{I(z)}{z}\right],
\end{aligned} \tag{8}$$

where

$$\begin{aligned}
I(z) &= 6\Big[\zeta_3 + 4\,{\rm Li}_3(-u) + 2\,{\rm Li}_3(u)\Big] - 8\Big[2\,{\rm Li}_2(-u) + {\rm Li}_2(u)\Big]\ln u - 2\Big[2\,\ln(1+u) + \ln(1-u)\Big]\ln^2 u\,,\\
G(z) &= \frac{2\,u\,\ln u}{u^2-1}\,, \quad \text{with} \quad u \equiv \frac{\sqrt{1-1/z}-1}{\sqrt{1-1/z}+1}\,.
\end{aligned} \tag{9}$$

An important application is the determination of the moments M_n in the fixed-order expansion. Here the pole mass scheme is strongly disfavored since it contains an $\mathcal{O}(\Lambda_{\rm QCD})$ renormalon ambiguity that leads to a quite bad perturbative expansion of the moments. For small values of n this problem can be avoided conveniently by using the $\overline{\rm MS}$ mass scheme. For the complications that arise for large values of n see e.g. Refs. [23, 24]. In this paper we use the $\overline{\rm MS}$ running mass $\overline{m}$ with $n_f = n_\ell + 1$ running flavors for discussions of the moments M_n. Using a common renormalization scale μ for the mass and the strong coupling, the fixed-order perturbative expansion of the moments M_n can be written in the form [$l_{m\mu} = \ln(\bar{m}^2(\mu)/\mu^2)$]

$$\begin{aligned}
M_n = \frac{9}{4}\,\frac{Q_q^2}{(4\bar{m}^2(\mu))^n}\Bigg[&\bar{C}_n^{(0)} + \frac{\alpha_s(\mu)}{\pi}\left(\bar{C}_n^{(10)} + \bar{C}_n^{(11)} l_{m\mu}\right) + \left(\frac{\alpha_s(\mu)}{\pi}\right)^2\left(\bar{C}_n^{(20)} + \bar{C}_n^{(21)} l_{m\mu} + \bar{C}_n^{(22)} l_{m\mu}^2\right)\\
&+ \left(\frac{\alpha_s(\mu)}{\pi}\right)^3\left(\bar{C}_n^{(30)} + \bar{C}_n^{(31)} l_{m\mu} + \bar{C}_n^{(32)} l_{m\mu}^2 + \bar{C}_n^{(33)} l_{m\mu}^3\right)\Bigg],
\end{aligned} \tag{10}$$

adopting the notation of Refs. [7, 8].

III. THE METHOD

The expansions of $\Pi(z)$ in the threshold region $z \simeq 1$ and the high-energy limit $|z| \to \infty$ involve powers of $\log(1-z)$ and $\log(-4z)$, respectively. Above production threshold for $z > 1$ these logarithmic terms contribute to the absorptive parts in Π that constitute the cross section according to Eq. (4). On the other hand, the expansion around $z = 0$, which is located in the Euclidean region, leads to fully analytic terms and admits a usual Taylor expansion. We want to reconstruct the full q^2 and mass dependence of $\Pi^{(3)}$ by building functions that incorporate all known properties of $\Pi^{(3)}$ in the threshold regime, the high-energy limit and the region around $z = 0$. We carry out the same program also for $\Pi^{(2)}$ using only coefficients in the expansions that are analogous to the available information for $\Pi^{(3)}$. From the reconstructed $\Pi^{(3)}$ we can determine previously unknown non-logarithmic coefficients in the high-energy and the nonrelativistic expansions as well as the $\mathcal{O}(\alpha_s^3)$ corrections of the moments M_n for $n \geq 3$. Using the reconstructed $\Pi^{(2)}$ function we can test the reliability of these determinations and find that these coefficients and moments can be determined remarkably well.

Following the approach of Ref. [7], we split $\Pi^{(2,3)}(z)$ into two parts,

$$\Pi^{(2,3)}(z) = \Pi^{(2,3)}_{\rm reg}(z) + \Pi^{(2,3)}_{\rm log}(z)\,, \tag{11}$$

where $\Pi^{(2,3)}_{\rm log}(z)$ are designed such that they contain the logarithmic terms in the expansions around $z = 1$ and for $|z| \to \infty$. They can be conveniently constructed from the functions $\Pi^{(1)}$ and $G(z)$ given in Eqs. (8) and (9) since the latter readily incorporate analytic structures that allow to incorporate the appropriate threshold and high-energy behavior into $\Pi^{(2,3)}_{\rm log}(z)$. Once $\Pi^{(2,3)}_{\rm log}(z)$ has been specified, the remaining task is to construct a Padé approximant for $\Pi^{(2,3)}_{\rm reg}$ that allows to incorporate the remaining non-logarithmic constraints in the regions $z \simeq 1$, $|z| \to \infty$ and $z \simeq 0$. The general structure of a Padé approximant $P_{n,m}$ has the form

$$P_{n,m}(x) \,=\, \frac{\sum_{i=0}^{n} a_i x^i}{1+\sum_{j=1}^{m} b_j x^j}\,, \tag{12}$$

which means that there are $n + m + 1$ coefficients that need to be specified. Note that the coefficients a_i and b_j are real numbers. Since $\Pi^{(2,3)}_{\rm reg}$ still has a physical cut for $z > 1$ along the positive real z axis, one cannot use the variable z to formulate the Padé approximant. A convenient variable to automatically account for this cut is ω defined by (see e.g. Refs. [17, 18])

$$\omega \,=\, \frac{1-\sqrt{1-z}}{1+\sqrt{1-z}}, \qquad\qquad z \,=\, \frac{4\omega}{(1+\omega)^2}. \tag{13}$$

Here, the physical z-plane is mapped into the unit-circle of the complex ω-plane, where approaching the physical cut from the upper (lower) complex z-half-plane corresponds to approaching the upper (lower) semi unit-circle in the complex ω-plane. The three points $z = (0, 1, \pm\infty)$ are conformally mapped onto $\omega = (0, 1, -1)$. Expressed in terms of the variable ω, $\Pi^{(2,3)}_{\rm reg}$ can therefore be approximated by rational functions involving the Padé approximant $P_{n,m}(\omega)$. All Padé approximants that turn out to have unphysical poles inside the unit circle have to be discarded. In practice some additional restrictive criteria have to be imposed to avoid an unphysical behavior of Π and R due to poles in the Padé approximant outside the unit circle that are either close to the unit circle or have a large residue. We discuss these restrictions in Sec. VI.

It goes without saying that the constructions of $\Pi^{(2,3)}_{\rm log}(z)$ and the Padé approximant for $\Pi^{(2,3)}_{\rm reg}$ are not unique and that the resulting reconstructed $\Pi^{(2,3)}$ functions have a dependence on choices made for their construction. The ambiguity in the procedure therefore needs to be quantified by accounting for variations in the construction. While in Ref. [7, 8] variations coming from different choices for $P_{n,m}$ were included for the error estimate, we include in our work in addition continuous variations in the construction of $\Pi^{(2,3)}_{\rm log}$. We test the reliability of the method by determining properties of $\Pi^{(2)}$ that are precisely known analytically, but that have not been incorporated for the construction of the approximation for $\Pi^{(2)}$.

IV. DESIGNING $\Pi_{\rm log}$

To determine $\Pi^{(2,3)}_{\rm log}$ we need to account for the logarithmic terms that arise in $\Pi^{(2,3)}$ in the threshold region $z \to 1$ and in the high-energy limit $|z| \to \infty$. To facilitate the presentation it is convenient to write

$$\Pi^{(2,3)}_{\rm log}(z) \,=\, \Pi^{(2,3)}_{\rm thr}(z) \,+\, \Pi^{(2,3)}_{\rm inf}(z) \,+\, \Pi^{(2,3)}_{\rm zero}(z)\,, \tag{14}$$

where $\Pi^{(2,3)}_{\rm thr}$ and $\Pi^{(2,3)}_{\rm inf}$ are designed to account for the logarithmic terms at threshold and at high energies, respectively, and $\Pi^{(2,3)}_{\rm zero}$ incorporates subtractions that ensure a physical behavior at $z = 0$.

Threshold Logarithms. We start by presenting the expansions of $\Pi^{(1,2,3)}(z)$ and $G(z)$ in the threshold limit $z \to 1$ keeping terms up to NNLO in the expansion in $\sqrt{1-z}$:

$$\begin{aligned}
\Pi^{(1)}(z) \;=\; & -0.1875\ln(1-z) - 0.314871 + 0.477465\sqrt{1-z} \\
& + \Big(0.354325 + 0.125\ln(1-z)\Big)(1-z) + \mathcal{O}\Big((1-z)^{3/2}\Big)\,, \\
\Pi^{(2)}(z) \;=& \frac{1.72257}{\sqrt{1-z}} + (0.34375 - 0.0208333 n_\ell)\ln^2(1-z) + (0.0116822 n_\ell + 1.64058)\ln(1-z) + K^{(2)} \\
& + \Big(-0.721213 - 0.0972614 n_\ell + 3.05433\ln(1-z)\Big)\sqrt{1-z} \;+\; \mathcal{O}\Big((1-z)\Big)\,, \\
\Pi^{(3)}(z) \;=& \frac{2.63641}{1-z} + \frac{0.678207 n_\ell - 27.2677}{\sqrt{1-z}} + (0.57419 n_\ell - 9.47414)\,\frac{\log(1-z)}{\sqrt{1-z}} \\
& + (-0.00231481 n_\ell^2 + 0.0763889 n_\ell - 0.630208)\log^3(1-z) \\
& + (0.00194703 n_\ell^2 + 0.0312341 n_\ell + 1.3171)\log^2(1-z) \\
& + (-0.0690848 n_\ell^2 + 2.37068 n_\ell - 17.6668)\log(1-z) \;+\; K^{(3)} + \mathcal{O}\Big((1-z)^{1/2}\Big)\,, \\
G(z) \;=& \frac{\pi}{2\sqrt{1-z}} - 1 + \frac{\pi\sqrt{1-z}}{4} \;+\; \mathcal{O}\Big((1-z)\Big)\,.
\end{aligned} \tag{15}$$

To avoid cluttering we show the various coefficients for $\Pi^{(1,2,3)}(z)$ in numerical form, but keep the number n_ℓ of light quark flavors as a variable. The expansions of $\Pi^{(1)}$ and G are known from their exact expressions given in Eqs. (8) and (9) while the expansion for $\Pi^{(2)}$ can be derived from the results for R in the threshold region computed in Ref. [25]. The expansion for $\Pi^{(3)}$ is obtained from the NNLO threshold cross section factorization formula for R within NRQCD first derived in Ref. [12, 13] (see also Ref. [26]). The result was later confirmed by many other groups [27]. Note that within NRQCD it is the standard convention that only the n_ℓ light quark species contribute to the running of the strong coupling. Switching to $n_f = n_\ell + 1$ running flavors affects the coefficient of the term $\propto \ln(1-z)$ in $\Pi^{(3)}$. All other coefficients shown in Eq. (15) are unaffected. We also note that the singlet contributions to the vacuum polarization function only affect the threshold expansion at N^{4}LO in the expansion in $\sqrt{1-z}$ and do not contribute at the order we consider here.[1] The constant terms $K^{(2,3)}$ that appear in the nonrelativistic expansion of $\Pi^{(2,3)}$ have not yet been computed from Feynman diagrams. As we show in Secs. VII and VIII they can be determined from the reconstructed vacuum polarization function based on the method described in Sec. III.

$\ln^m(1-z)$	$[\Pi^{(1)}(z)]^m$
$(1-z)^{-n/2}\ln^m(1-z)$	$[G(z)]^n[\Pi^{(1)}(z)]^m$
$(1-z)^{n/2}\ln^m(1-z)$	$(1-z)^n[G(z)]^n[\Pi^{(1)}(z)]^m$

TABLE I: First column: Logarithmic terms that arise in the expansion of $\Pi^{(2,3)}(z)$ close to threshold where $z \approx 1$. Second column: Corresponding functions used in the construction of $\Pi^{(2,3)}_{\rm thr}(z)$.

To construct $\Pi^{(2,3)}_{\rm thr}$ we have to find appropriate functions that account for the different combinations of the logarithmic term $\ln(1-z)$ and powers of $\sqrt{1-z}$ that appear in Eqs. (15). A convenient choice is given in Tab. I, and leads to

$$\begin{aligned}
\Pi^{(2)}_{\rm thr}(z) \;=\; & A_0^{(2)}\,\frac{1+a_0^{(2)}\,z}{z}\left[\Pi^{(1)}(z)\right]^2 + A_1^{(2)}\Pi^{(1)}(z) + A_2^{(2)}(1-z)G(z)\Pi^{(1)}(z)\,, \\
\Pi^{(3)}_{\rm thr}(z) \;=\; & A_0^{(3)}\,\frac{1+a_0^{(3)}\,z}{z}\left[\Pi^{(1)}(z)\right]^3 + A_1^{(3)}\left[\Pi^{(1)}(z)\right]^2 + A_2^{(3)}\,\frac{1+a_2^{(3)}\,z}{z}G(z)\Pi^{(1)}(z) + A_3^{(3)}\Pi^{(1)}(z)\,.
\end{aligned} \tag{16}$$

[1] Within NRQCD the dominant effect of the singlet contributions is associated to 4-quark operators with a Wilson coefficient that incorporates the hard effects of the 3-gluon annihilation. This operator leads to a momentum space potential $\propto \alpha_s^3/m^2$.

The coefficients $A_i^{(2,3)}$ can be unambiguously determined from the expressions shown in Eqs. (15). Obviously the choices in Tab. I are not unique. To have some quantitative way to account for this source of uncertainty we have multiplied the functions related to the highest power of $\ln(1-z)$ in different orders in the expansion in $\sqrt{1-z}$ by a term $(1-a_i^{(2,3)}\,z)/z$, where the $a_i^{(2,3)}$ are free parameters. Since the construction becomes singular for $a_i^{(2,3)} = -1$, we exclude this value and use variations in the ranges $a_i^{(2,3)} \geq 0$ and $a_i^{(2,3)} \leq -2$. Note that for $|a_i^{(2,3)}| \to \infty$ the term $(1-a_i^{(2,3)}\,z)/z$ becomes z-independent and the results for $\Pi_{\rm thr}^{(2,3)}$ become independent of the $a_i^{(2,3)}$. We note that given the functions in Tab. I it is straightforward to account for even higher terms in the expansion in the threshold limit for the construction of $\Pi_{\rm thr}^{(2,3)}$.

High-Energy Logarithms. The expansions of $\Pi^{(1,2,3)}(z)$ and $G(z)$ in the high-energy limit $|z| \to \infty$ read

$$
\begin{aligned}
\Pi^{(1)}(z) \;=\; & -\,0.018998\log(-4z) - 0.075514 - 0.056993\frac{\ln(-4z)}{z} \\
& + \frac{0.023628}{z^2} - 0.014248\frac{\ln^2(-4z)}{z^2} - 0.011874\frac{\ln(-4z)}{z^2} + \mathcal{O}(z^{-3})\,, \\
\Pi^{(2)}(z) \;=\; & (0.034829 - 0.0021109 n_f)\ln^2(-4z) + (-0.050299 + 0.0029205 n_f)\ln(-4z) + H_0^{(2)} \\
& + (0.18048 - 0.0063326 n_f)\frac{\ln^2(-4z)}{z} + (-0.59843 + 0.027441 n_f)\frac{\ln(-4z)}{z} + \frac{H_1^{(2)}}{z} \\
& + (0.042745 - 0.0010554 n_f)\frac{\ln^3(-4z)}{z^2} + (-0.10132 + 0.0058049 n_f)\frac{\ln^2(-4z)}{z^2} \\
& + (-0.48134 + 0.032065 n_f)\frac{\ln(-4z)}{z^2} + \frac{H_2^{(2)}}{z^2} + \mathcal{O}(z^{-3})\,, \\
\Pi^{(3)}(z) \;=\; & (-0.063853 + 0.0077398 n_f - 0.00023454\; n_f^2)\ln^3(-4z) \\
& + (0.21906 - 0.026441 n_f + 0.0004867 n_f^2)\ln^2(-4z) \\
& + (-0.46209 + 0.10679 n_f - 0.0021837 n_f^2)\ln(-4z) + H_0^{(3)} \\
& + (-0.45120 + 0.035885 n_f - 0.00070362 n_f^2)\frac{\ln^3(-4z)}{z} + (3.0848 - 0.26016 n_f + 0.0045735 n_f^2)\frac{\ln^2(-4z)}{z} \\
& + (-6.6516 + 0.78237 n_f - 0.0146587 n_f^2)\frac{\ln(-4z)}{z} + \frac{H_1^{(3)}}{z} \\
& + (-0.10152 + 0.0060687 n_f - 0.000087952 n_f^2)\frac{\ln^4(-4z)}{z^2} \\
& + (0.57013 - 0.044856 n_f + 0.0006743 n_f^2)\frac{\ln^3(-4z)}{z^2} + (0.17822 + 0.038525 n_f - 0.00088394 n_f^2)\frac{\ln^2(-4z)}{z^2} \\
& + (-8.8712 + 1.0393 n_f - 0.026019 n_f^2)\frac{\ln(-4z)}{z^2} + \frac{H_2^{(3)}}{z^2} + \mathcal{O}(z^{-3})\,, \\
G(z) \;=\; & -\frac{\log(-4z)}{2z} + \frac{1-\log(-4z)}{4z^2} + \mathcal{O}(z^{-3})\,.
\end{aligned}
\tag{17}
$$

The expansions for $\Pi^{(1)}$ and G are known from the exact expressions given in Eqs. (8) and (9), while the expansion for $\Pi^{(2)}$ was taken from Ref. [28]. Note that many orders in high-energy expansion are known for $\Pi^{(2)}$ [29], but we only consider in this work terms up to order $1/z^2$, since our analysis for $\Pi^{(2)}$ mainly serves as a testing ground for the application to $\Pi^{(3)}$. The expansion for $\Pi^{(3)}$ was obtained in Refs. [10]. At $\mathcal{O}(\alpha_s^2)$ the non-logarithmic coefficients $H_{0,1}^{(2)}$ are known analytically [8] and read

$$
\begin{aligned}
H_0^{(2)} \;&=\; -\,0.73628 + 0.037645 n_f\,, \\
H_1^{(2)} \;&=\; -\,0.30324 + 0.029002 n_f\,.
\end{aligned}
\tag{18}
$$

At $\mathcal{O}(\alpha_s^3)$ the non-logarithmic coefficients $H_{0,1}^{(3)}$ have not been computed from Feynman diagrams in the literature before. As we show in Secs. VII and VIII they can be determined from the reconstructed vacuum polarization function $\Pi^{(3)}$.

$\ln^n(-4z)$	$(1-z)^n\,[G(z)]^n$
$\frac{1}{z}\ln^n(-4z)\,,(n>1)$	$(1-z)^{n-1}\,[G(z)]^n$
$\frac{1}{z}\ln(-4z)$	$\frac{1-z}{z}\,G(z)$
$\frac{1}{z^2}\ln(-4z)$	$\frac{1-z}{z^2}\,G(z)$
$\frac{1}{z^2}\ln^2(-4z)$	$\frac{1-z}{z}\,[G(z)]^2$
$\frac{1}{z^2}\ln^3(-4z)$	$\frac{(1-z)^2}{z}\,[G(z)]^3$
$\frac{1}{z^2}\ln^4(-4z)$	$(1-z)^2\,[G(z)]^4$

TABLE II: First column: Logarithmic terms that arise in the high-energy expansion of $\Pi^{(2,3)}(z)$ where $|z|\to\infty$. Second column: Corresponding functions used in the construction of $\Pi_{\rm inf}^{(2,3)}(z)$.

To construct $\Pi_{\rm inf}^{(2,3)}(z)$ we have to find functions that can account for the different combinations of powers of $\ln(-4z)$ and of powers of $1/z$ that arise in the expansions of Eq. (17). A convenient choice is given in Tab. II. Our guideline for including the factors of $(1-z)^i$ is to ensure that the functions are constant or $\sim\sqrt{1-z}$ in the threshold limit $z\to 1$. This leads to

$$\begin{aligned}
\Pi_{\rm inf}^{(2)} =& B_0^{(2)}\frac{1+b_0^{(2)}z}{z}(1-z)^2G(z)^2+\left(B_{10}^{(2)}+\frac{B_{11}^{(2)}}{z}\right)\frac{1+b_1^{(2)}z}{z}(1-z)G(z)^2\\
&+\left(B_{30}^{(2)}+\frac{B_{31}^{(2)}}{z}+\frac{B_{32}^{(2)}}{z^2}\right)(1-z)G(z)+B_4^{(2)}\frac{(1-z)^2}{z}G(z)^3,\\
\Pi_{\rm inf}^{(3)} =& \frac{1+b_0^{(3)}z}{z}\left(B_{00}^{(3)}+\frac{B_{01}^{(3)}}{z}\right)(1-z)^3G(z)^3+B_1^{(3)}(1-z)^2G^4(z)+\frac{1+b_2^{(3)}z}{z}\left(B_{20}^{(3)}+\frac{B_{21}^{(3)}}{z}\right)(1-z)^2G(z)^3\\
&+B_{30}^{(3)}(1-z)^2G(z)^2+\left(B_{40}^{(3)}+\frac{B_{41}^{(3)}}{z}\right)(1-z)G(z)^2+\left(B_{50}^{(3)}+\frac{B_{51}^{(3)}}{z}+\frac{B_{52}^{(3)}}{z^2}\right)(1-z)G(z)\,,
\end{aligned}\tag{19}$$

where the coefficients $B_i^{(n)}$ can be determined unambiguously from the conditions in Eqs. (15) and (17). In analogy to $\Pi_{\rm thr}^{(2,3)}$ we have included modification factors $(1+b_i^{(2,3)}\,z)/z$ for the functions that are related to highest-power logarithmic terms at each order in the $1/z$ expansion. In $\Pi_{\rm high}^{(3)}$ we have a common modification factor for the functions related to the terms $\ln^3(-4z)/z$ and $\ln^3(-4z)/z^2$. For the parameters $b_i^{(2,3)}$ the choice $b_i^{(2,3)}=0$ is excluded because in this case the construction becomes singular. For our analysis we adopt variations in the ranges $|b_i^{(2,3)}|\geq 1$. Using functions along the lines of Tab. I it is straightforward to account for even higher terms in the high-energy expansion in the for the construction of $\Pi_{\rm inf}^{(2,3)}$.

Note that for the determination of the coefficient $A_i^{(2,3)}$ and $B_i^{(2,3)}$ one first fixes the constants $a_i^{(2,3)}$ and $b_i^{(2,3)}$ in the modification functions and then solves a set of linear equations.

Subtractions at $q^2=0$. There are singularities $\sim 1/z$ and $\sim 1/z^2$ in $\Pi_{\rm thr}^{(2,3)}(z)$ and $\Pi_{\rm inf}^{(2,3)}(z)$ that arise in the limit $z\to 0$. They are a consequence of the functions used to construct $\Pi_{\rm thr}^{(2,3)}(z)$ and $\Pi_{\rm inf}^{(2,3)}(z)$. These singularities lead to unphysical behavior and need to be subtracted. For this task we define the function

$$\Pi_{\rm zero}^{(2,3)}(z)\;=\;S_0^{(2,3)}\;+\;\frac{S_1^{(2,3)}}{z}\;+\;\frac{S_2^{(2,3)}}{z^2}\,.\tag{20}$$

After the coefficients $A_i^{(2,3)}$ and $B_i^{(2,3)}$ have been computed, the coefficients $S_{0,1,2}^{(2,3)}$ are determined such that

$$\Pi_{\rm log}^{(2,3)}(0) \,=\, 0\,. \tag{21}$$

Note that it is not mandatory to fix $S_0^{(2,3)}$ in this way, and that our approach is independent of the choice for $S_0^{(2,3)}$. However, to satisfy Eq. (6) it is convenient for the purpose of presentation to impose the condition (21) and also the relation $\Pi_{\rm reg}^{(2,3)}(0) = 0$.

V. DESIGNING $\Pi_{\rm reg}$

The terms $\Pi_{\rm reg}^{(2,3)}$ in Eq. (11) have to account for the non-logarithmic conditions in the expansion at the threshold and at high energies, and for the coefficients that arise in the expansion around $z = 0$. We start by presenting the small-z expansion of $\Pi^{(2)}$ and $\Pi^{(3)}$:

$$\begin{aligned}
\Pi^{(2)} \,=&(0.719976 - 0.0296233 n_\ell) z + (0.698894 - 0.0275334 n_\ell) z^2 + (0.637986 - 0.0240088 n_\ell) z^3 \\
&+ (0.584109 - 0.0211621 n_\ell) z^4 + (0.539450 - 0.0189263 n_\ell) z^5 + (0.502392 - 0.0171420 n_\ell) z^6 \\
&+ (0.471258 - 0.0156884 n_\ell) z^7 + \mathcal{O}(z^8)\,, \\
\Pi^{(3)} \,=&(10.6103 - 1.30278 n_\ell + 0.0282783 n_\ell^2) z + (10.4187 - 1.12407 n_\ell + 0.0223706 n_\ell^2) z^2 \,+\, \mathcal{O}(z^3)\,.
\end{aligned} \tag{22}$$

The coefficients for $\Pi^{(2)}$ were computed in Refs. [7, 8]. Recently the coefficients for $\Pi^{(2)}$ have even been determined up to order z^{30} [30, 31]. For $\Pi^{(3)}$ the coefficient of order z was computed in Refs. [14, 15], and the coefficient of order z^2 was given in Ref. [16]. The coefficients of order z^n with $n \geq 3$ have not yet been computed from Feynman diagrams. However, they can be determined from the reconstructed function $\Pi^{(3)}$ as we show in Secs. VII and VIII.

Designing $\Pi_{\rm reg}^{(2)}$. We start exemplarily with the construction of $\Pi_{\rm reg}^{(2)}$. Close to threshold $\Pi^{(2)}$ exhibits the Coulomb singularity $\sim 1/\sqrt{1-z}$, see Eq. (15). To avoid that the Padé approximant contains explicitly this singularity, we use two different methods:

(i) We relate the Padé approximant $P(\omega)$ to $f(z)\Pi_{\rm reg}^{(2)}$, where $f(z \approx 1) \sim \sqrt{1-z}$. The coefficient of the Coulomb singularity is implemented through a condition on $P(1)$.

(ii) We use the relation

$$\frac{\pi^2}{9}\, G(z \approx 1) \,=\, \frac{\pi^3}{18\sqrt{1-z}} \,+\, \ldots \tag{23}$$

and account for the Coulomb singularity by adding the function $\frac{\pi^2}{9} G(z)$ to $\Pi_{\rm log}^{(2)}$. The Padé approximant P is not affected by the Coulomb singularity.

The numerical differences that result from these two methods of implementing the Coulomb singularity constitute another tool for quantifying the uncertainties inherent to our approach.

For method (i) the expression we use for the relation between the Padé approximant $P(\omega)$ and $\Pi_{\rm reg}^{(2)}$ reads

$$P(\omega) \,=\, \frac{1-\omega}{(1+\omega)^2} \left[\Pi_{\rm reg}^{(2)}(z) - \Pi_{\rm reg}^{(2)}(-\infty)\right], \tag{24}$$

where $\frac{1-\omega}{(1+\omega)^2} \sim \sqrt{1-z}$ for $z \to 1$. A similar relation was also used in Ref. [8]. Since the prefactor grows linearly with z, $P(-1)$ is a finite number. Some comments are in order concerning the term $\Pi_{\rm reg}(-\infty)$ that appears in Eq. (24) and also in the analogous relations (27) and (29) that follow below. From the conditions $\Pi(0) = \Pi_{\rm log}(0) = \Pi_{\rm reg}(0) = 0$ it is easy to see that

$$P(0) \,=\, -\,\Pi_{\rm reg}(-\infty)\,. \tag{25}$$

Thus in case that $\Pi_{\rm reg}(-\infty)$ is known and taken as an input, Eq. (25) represents a condition that is imposed on the Padé approximant P. On the other hand, if $\Pi_{\rm reg}(-\infty)$ is unknown or not taken as an input, it can be determined from Eq. (25) once the Padé approximant has been fixed from other conditions. We show in Secs. VII and VIII that this allows to determine the high energy constants $H_0^{(2,3)}$ with small uncertainties. From Eqs. (24), (25) and (11) the vacuum polarization function $\Pi^{(2)}$ is recovered from the relation

$$\Pi^{(2)}(z) \,=\, \frac{(1+\omega)^2}{1-\omega}\,P(\omega) \,-\, P(0) \,+\, \Pi^{(2)}_{\rm log}(z)\,. \tag{26}$$

From Eqs. (24) it is now straightforward to determine the conditions on the Padé approximant $P(\omega)$ from the non-logarithmic constraints on $\Pi(z)$ in the threshold and the high-energy regions and from the coefficients in the expansion around $z = 0$. Additional constraints on P arise from the fact that in the limit $|z| \to \infty$ the first term on the RHS of Eq. (26) can exhibit odd power terms $\sim 1/z^{(2n+1)/2}$ with $n = 1, 2, \ldots$, which do not exist in the high-energy expansion of the vacuum polarization function. It is reasonable to exclude such terms up to order $1/z^{(2n+1)/2}$ when the information from the high-energy expansion up to order $1/z^n$ is accounted for. For example, excluding terms $\sim 1/z^{3/2}$ in Eq. (26) leads to the constraint $P(-1) - 2P'(-1) = 0$, where P' refers to the derivative of $P(\omega)$ with respect to ω. Excluding also terms $\sim 1/z^{5/2}$ leads to the condition $3P(-1) - 9P''(-1) + 2P'''(-1) = 0$. The various conditions on P lead to a complicated non-linear set of equations for the coefficients of the Padé approximant in Eqs. (12), which we do not present explicitly here. These equations frequently have multiple solutions and are most conveniently tackled numerically.

For method (ii), where the Coulomb singularity is treated in $\Pi^{(2)}_{\rm log}$ the relation between the Padé approximant $P(\omega)$ and $\Pi^{(2)}_{\rm reg}(z)$ reads

$$P(\omega) \,=\, \frac{1}{(1+\omega)^2}\left[\Pi^{(2)}_{\rm reg}(z) - \Pi^{(2)}_{\rm reg}(-\infty)\right]. \tag{27}$$

A similar relation was also used in Ref. [8]. Here, excluding terms of order $1/z^{3/2}$ and $1/z^{5/2}$ for $|z| \to \infty$ corresponds to the conditions $P(-1) - P'(-1) = 0$ and $6P(-1) - 6P''(-1) + P'''(-1) = 0$, respectively. The vacuum polarization function is then recovered from the relation

$$\Pi^{(2)}(z) \,=\, (1+\omega)^2\,P(\omega) \,-\, P(0) \,+\, \Pi^{(2)}_{\rm log}(z)\,. \tag{28}$$

Designing $\Pi^{(3)}_{\rm reg}$. The construction of $\Pi^{(3)}_{\rm reg}$ proceeds in a similar way. At $\mathcal{O}(\alpha_s^3)$ the vacuum polarization function has a Coulomb singularity $\sim 1/(1-z)$. For method (i) this singularity is incorporated in $\Pi^{(3)}_{\rm reg}$ and the relation between $P(\omega)$ and $\Pi^{(3)}_{\rm reg}$ reads

$$P(\omega) \,=\, \left(\frac{1-\omega}{1+\omega}\right)^2\left[\Pi^{(3)}_{\rm reg}(z) - \Pi^{(3)}_{\rm reg}(-\infty)\right], \tag{29}$$

where $(1-\omega)^2 \sim (1-z)$ for $z \to 1$. Excluding terms of order $1/z^{3/2}$ and $1/z^{5/2}$ for $|z| \to \infty$ corresponds to the conditions $P'(-1) = 0$ and $3P''(-1) - P'''(-1) = 0$, respectively. The vacuum polarization function is recovered from the relation

$$\Pi^{(3)}(z) \,=\, \left(\frac{1+\omega}{1-\omega}\right)^2\,P(\omega) \,-\, P(0) \,+\, \Pi^{(3)}_{\rm log}(z)\,. \tag{30}$$

For method (ii) we add the function $8\zeta_3[G(z)]^2/9$ to $\Pi^{(3)}_{\rm log}$. Since $8\zeta_3[G(z)]^2/9 \to 2\,\pi^2\zeta_3/[9(1-z)]$ for $z \to 1$ the Coulomb singularity is therefore accounted for in $\Pi^{(3)}_{\rm log}$. The relation between the Padé approximants and $\Pi^{(3)}_{\rm reg}$ has then the same form as Eq. (24) with $\Pi^{(2)}_{\rm reg}$ replaced by $\Pi^{(3)}_{\rm reg}$. The relation for the $\Pi^{(3)}(z)$ has the same form as Eq. (26) with $\Pi^{(2)}_{\rm log}$ replaced by $\Pi^{(3)}_{\rm log}$. The relations imposed on P to exclude terms of order $1/z^{3/2}$ and $1/z^{5/2}$ are then also $P(-1) - 2P'(-1) = 0$ and $3P(-1) - 9P''(-1) + 2P'''(-1) = 0$, respectively.

VI. DISCARDING UNPHYSICAL SOLUTIONS

For the reconstructed functions $\Pi^{(2)}$ and $\Pi^{(3)}$ we have several types of variations that can be implemented into the construction and which we can use to quantify numerically the uncertainty of the results. Apart from the two ways to account for the Coulomb singularity described as methods (i) and (ii) in the previous section, we have also implemented modification factors in Eqs. (16) and (19) that allow us to scan over a continuous set of functions within $\Pi_{\rm log}^{(2,3)}$. Once the modification functions are fixed there are in general several possible choices one can use for the Padé approximants $P_{m,n}$ with $n+m$ being fixed by the number of conditions one imposes on $\Pi_{\rm reg}^{(2,3)}$. The resulting solutions for the Padé approximants can, however, have properties that lead to an unphysical and pathological behavior for Π and R. Such solutions need to be discarded for a meaningful phenomenological analysis [8].

An obvious restriction concerns solutions for $P_{m,n}(\omega)$ that lead to poles in $\Pi^{(2,3)}$ in the complex ω-plane inside the unit circle.[2] These solutions are unacceptable and we discard them right away because such poles lead to an unphysical analytic structure. A more subtle situation arises for solutions with poles in $\Pi^{(2,3)}$ in the upper complex ω-half-plane that are outside the unit circle, but are either close to the unit circle or have a large residue. Although the analytic structure of such solutions is not a priori wrong, we still discard such solutions if they lead to an unphysical resonance-like structure in the cross section R. To have a quantitative criterion that can be implemented easily automatically we compute for every pole in $\Pi_{\rm reg}$ in the upper complex ω-half-plane the so called *pole factor*

$$\rho = \frac{|{\rm Res}_\Pi(\omega_{\rm pole})|}{|\omega_{\rm pole}| - 1}\,, \tag{31}$$

where $\omega_{\rm pole}$ is the location of the pole in the complex ω-plane and ${\rm Res}_\Pi(\omega_{\rm pole})$ the residue of $\Pi^{(2,3)}$ at $\omega_{\rm pole}$. If $|\omega_{\rm pole}|$ is close to unity or if the residue is large, the pole factor becomes big and a resonance-like structure can arise in R. We discard solutions when $\rho > \rho_0$. For our analysis we found that the choice $\rho_0 = 2.8$ represents a reasonable restriction for $\Pi^{(2)}$, while for $\Pi^{(3)}$ we use $\rho_0 = 30$. For the vacuum polarization function $\Pi^{(3)}$ a larger value for ρ_0 is used since such poles arise predominantly in the threshold region close to $\omega = 1$. Here ${\rm Im}[\Pi^{(3)}]$ is substantially larger than ${\rm Im}[\Pi^{(2)}]$ due to the bigger size of its Coulomb singularity, see Eq. (15). Given the set of solutions for $\Pi^{(2)}$ that pass the restrictions described above we can analyze how well these solutions reproduce other well-known properties of $\Pi^{(2)}$.

VII. ANALYSIS FOR THE VACUUM POLARIZATION AT $\mathcal{O}(\alpha_s^2)$

The purpose of this section is two-fold. First we demonstrate the reliability of our approach for its application to $\Pi^{(3)}$ by testing it with the rather well-known $\mathcal{O}(\alpha_s^2)$ vacuum polarization function $\Pi^{(2)}$ and, second, we determine the previously unknown constant $K^{(2)}$ that appears in the nonrelativistic expansion of $\Pi^{(2)}$ close to the threshold, see Eq. (15).

To demonstrate the reliability of our approach let us reconstruct $\Pi^{(2)}$ using only information from the different expansions that is analogous to the available information in $\Pi^{(3)}$. Thus we account for the expansions in the threshold region up to NNLO, in the high-energy region up to order $1/z^2$ and up to order z^2 for the expansion around $z = 0$. For the construction of $\Pi_{\rm reg}^{(2)}$ this entails that we account for the first two coefficients of the expansion around $z = 0$, the non-logarithmic term $\propto \sqrt{1-z}$ in the threshold region and the constraints that terms $\sim 1/z^{3/2}$ and $\sim 1/z^{5/2}$ are absent for $|z| \to \infty$. We do not implement the known constants $H_{0,1}^{(2)}$, but we determine them from the reconstructed $\Pi^{(2)}$. This amounts to 6 constraints on the Padé approximant for method (i), where the Coulomb singularity is accounted for in $\Pi_{\rm reg}^{(2)}$, and to 5 constraints on the Padé approximant for method (ii), where the Coulomb singularity is accounted for in $\Pi_{\rm log}^{(2)}$. Thus we have $n + m = 5$ for the Padé approximants $P_{m,n}$ for method (i) and $n + m = 4$ for the Padé approximants for method (ii).

Given the analytic form for the reconstructed $\Pi^{(2)}$ functions we can expand them in the threshold region, the high-energy limit and around $q^2 = 0$. In Fig. 1 the results for the coefficients $\bar{C}_k^{(20)}$ for $k = 3, 4, 5, 6, 7$, the high-energy constants $H_{0,1}^{(2)}$ and the threshold constant $K^{(2)}$ are displayed exemplarily for $n_f = n_\ell + 1 = 4$ relevant for

[2] For Padé approximants of the form $P_{k,0}$ (Taylor-like) such poles do not exist and none of the solutions is discarded.

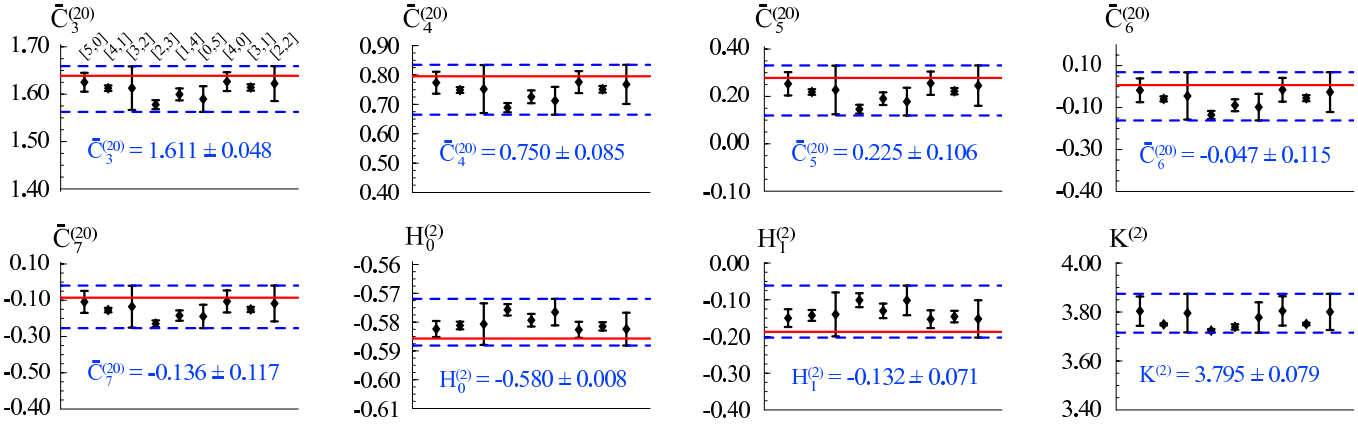

FIG. 1: Results from the reconstructed $\Pi^{(2)}$ function in approximation C for the coefficients $C^{(20)}_{3,4,5,6,7}$ that arise in the expansion around $z = 0$, for the coefficients $H^{(2)}_{0,1}$ that occur in the non-logarithmic terms in the high-energy expansion $|z| \to \infty$ and for the constant $K^{(2)}$ that appears in the expansion at threshold around $z = 1$. The red solid lines represent the respective exact results known from computation of Feynman diagrams. The dashed blue lines represent the envelope of all results obtained from the reconstructed $\Pi^{(2)}$ functions. The individual error bars represent the range of vales obtained from the reconstructed $\Pi^{(2)}$ functions using one particular Padé approximant $P_{m,n}$. The various types of Padé approximants that have been used are indicated in the upper left panel; the same order is used for all other panels. All results are for $n_f = n_\ell + 1 = 4$ running flavors relevant for charm production.

the production of charm quarks. The labels $[m, n]$ which have been added to the upper left panel for $\bar{C}_3^{(20)}$ refer to the Padé approximant used for the respective $\Pi^{(2)}_{\rm reg}$ functions, and their order is representative for all diagrams. The error bars represent the range of values covered by the variations of the modification factors as described in Sec. IV. The blue dashed lines indicate the range covered by all individual results and the red solid lines show the exact result obtained from Feynman diagrams. We see that for all cases the exact values are well within the range covered by the reconstructed $\Pi^{(2)}$ functions. Particularly precise determination are obtained for $\bar{C}_3^{(20)}$ and the leading high-energy coefficient $H_0^{(2)}$. We also obtain a very precise determination of the the threshold constant $K^{(2)}$.

	approx. A	approx. B	approx. C	approx. D	approx. E	exact
$\bar{C}_1^{(20)}$						2.49671
$\bar{C}_2^{(20)}$						2.77702
$\bar{C}_3^{(20)}$	1.365 ± 0.425	1.609 ± 0.266	1.611 ± 0.048			1.63882
$\bar{C}_4^{(20)}$	0.283 ± 0.799	0.770 ± 0.441	0.750 ± 0.085			0.79555
$\bar{C}_5^{(20)}$	-0.389 ± 1.057	0.271 ± 0.521	0.225 ± 0.106	0.278 ± 0.001		0.27814
$\bar{C}_6^{(20)}$	-0.744 ± 1.213	0.021 ± 0.541	-0.047 ± 0.115	0.007 ± 0.002		0.0070080
$\bar{C}_7^{(20)}$	-0.871 ± 1.296	-0.054 ± 0.528	-0.136 ± 0.117	-0.086 ± 0.003	-0.08594 ± 0.00003	-0.085963
$H_0^{(2)}$	0.159 ± 0.770	-0.561 ± 0.063	-0.580 ± 0.008	-0.5854 ± 0.0004	-0.5857 ± 0.0001	-0.58570
$H_1^{(2)}$	0.007 ± 0.574	0.338 ± 0.871	-0.132 ± 0.071	-0.180 ± 0.008	-0.185 ± 0.004	-0.18723
$K^{(2)}$	-6.64 ± 10.12	3.933 ± 0.303	3.795 ± 0.079	3.809 ± 0.032	3.805 ± 0.020	

TABLE III: Results for the coefficients $\bar{C}^{(20)}_{3,4,5,6,7}$, $H^{(2)}_{0,1}$ and $K^{(2)}$ from the reconstructed $\Pi^{(2)}$ functions using various different types of approximations for $\Pi^{(2)}$. Empty entries for coefficients $\bar{C}^{(20)}_k$ indicate that they are exact in that particular approximation. The exact analytic form for $K^{(2)}$ is unknown. All results are for $n_f = n_\ell + 1 = 4$ running flavors relevant for charm production.

To demonstrate that our approach is systematic we need to show that the results become more accurate once more information is included for the reconstruction of $\Pi^{(2)}$. In Tab. III the results of Fig. 1 for $\bar{C}^{(20)}_k$ with $k = 3, 4, 5, 6, 7$, $H^{(2)}_{0,1}$ and $K^{(2)}$ are displayed in the line labeled as "approximation C". In comparison we also show the results when all the information $\sim 1/z^2$ in the high-energy expansion is neglected for the reconstruction of $\Pi^{(2)}$ ("approximation B")

and when in addition to that also all NNLO threshold information is neglected ("approximation A"). The results show that the properties of the vacuum polarization can be determined more accurately once more information is used for its reconstruction with our approach. Moreover, we find that the variations of the reconstructed vacuum polarization function due to the different choices for the modification factors and the Padé approximants represent a reliable tool to estimate the uncertainties.

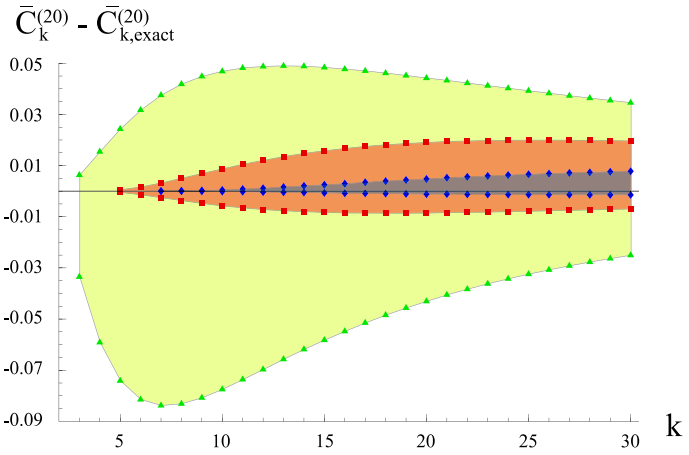

FIG. 2: Difference of the values for $\bar{C}_k^{(20)}$, determined from the reconstructed $\Pi^{(2)}$ functions based on Taylor-like Padé approximants, and the known exact values $\bar{C}_{k,\mathrm{exact}}^{(20)}$. The results are shown for approximation C (green triangles and light greed shaded area), D (red squared symbols and medium red shaded area) and E (blue diamonds and dark blue shaded area). The shaded areas represent the variation of the results due to the changes in the modification factors.

It is an astounding and amusing fact our approach allows for a determination of the coefficients $\bar{C}_k^{(20)}$ for large values of k with practically negligible uncertainties. This is demonstrated in Fig. 2 where the difference of the results we obtain for the coefficients $\bar{C}_k^{(20)}$ and the exact values from Ref. [30, 31], $\bar{C}_k^{(20)} - \bar{C}_{k,\mathrm{exact}}^{(20)}$ are shown up to $k = 30$. The range of values between the green triangular-shaped symbols (green light shaded region) is obtained from approximation C using solutions with Taylor-like Padé approximants. For $k > (10, 15, 20)$ the maximal relative discrepancy to the exact values is below $(14, 3, 1)\%$. The discrepancies become even smaller when more of the coefficients in the expansion around $z = 0$ of Eq. (22) are accounted for in the reconstruction of $\Pi^{(2)}$. Including the coefficients up to order z^4 (approximation D) we obtain the range of values between the red squared symbols (red shaded region). In this case we obtain for $k > (10, 15, 20)$ a maximal relative discrepancy to the exact values of below $(3, 0.8, 0.5)\%$. Including the coefficients up to order z^6 (approximation E) we obtain the range of values between the blue diamond-shaped symbols (blue dark shaded region). Here, we obtain for $k > 10$ a maximal relative discrepancy to the exact values of below 0.2%. The results for the high-energy coefficients $H_{0,1}^{(2)}$ for approximations D and E are also shown in Tab. III. Again we find agreement with the exact results with decreasing uncertainties once more information is included for the reconstruction of $\Pi^{(2)}$. Given the excellent quality of the results we consider our approach a reliable method to determine the previously unknown threshold constant $K^{(2)}$. As our final result for $K^{(2)}$ we adopt

$$K^{(2)} \;=\; 3.81 \;\pm\; 0.02\,. \tag{32}$$

To conclude this section let us analyze the $\mathcal{O}(\alpha_s^2)$ corrections to the e^+e^- cross section obtained from the reconstructed $\Pi^{(2)}$. In Fig. 3 we have plotted $12\pi v \mathrm{Im}[\Pi^{(2)}(q^2 + i0)]$ for $n_f = 4$ relevant for charm quark production in the pole mass scheme as a function of the quark velocity $v = \sqrt{1 - 1/z}$. We have included the factor of v to suppress the Coulomb $1/v$-singularity that arises in the cross section for small values of v and to have a finite value in the limit $v \to 0$. In the left panel the result for approximation C is shown. The red band is the area covered by all solutions for $\Pi^{(2)}$ that pass the criteria discussed in Sec. VI and represents the uncertainty. The size of the uncertainty corresponds to the envelope of the individual error bars shown in Fig. 1 where approximation C has been used as well. For comparison we have also displayed the expansions in the threshold region for $v \to 0$ (dotted lines) and in the high-energy limit for $v \to 1$ (dashed lines), where the short lines refer to leading order, the medium-length lines to next-to-leading order and the longest lines to next-to-next-to-leading order. The uncertainties are reduced substantially when additional coefficients for the expansion around $z = 0$ are included for the reconstruction of $\Pi^{(2)}$. This is demonstrated in the right panel, where the coefficients up to order z^6 are included for the reconstruction of $\Pi^{(2)}$. Again the red band

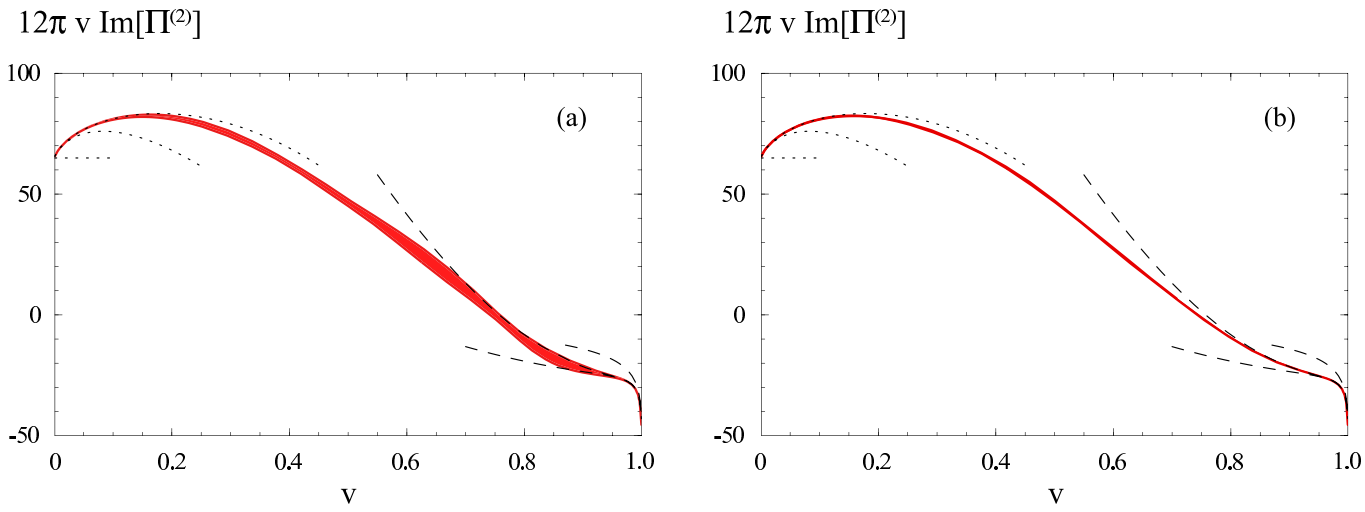

FIG. 3: Results for $12\pi v\mathrm{Im}[\Pi^{(2)}(q^2+i0)]$ as a function of v for $n_f = 4$. The red bands represent the uncertainties. In the left panel the results are based on the reconstructed $\Pi^{(2)}$ function incorporating the coefficients in the small-z expansion up to order z^2 (approximation C) and in the right panel the coefficients up to order z^6 are accounted for. The dotted and dashed black lines show the expansions in the threshold and the high-energy region up to NNLO. See the text for more details.

is the area covered by all solutions for $\Pi^{(2)}$ that pass the criteria discussed in Sec. VI. For method (i) to account the Coulomb singularity we found solutions based on the Padé approximants [9,0], [8,1], [7,2], [6,3], [5,4], [3,6], [1,8], and for method (ii) we found solutions based on the Padé approximants [8,0], [7,1], [6,2], [5,3], [4,4], [3,5], [1,7]. The width of the band is already smaller than the width of the solid lines used to draw the boundaries of the band. For $v = (0.2, 0.4, 0.6, 0.8)$ the relative uncertainty is $\pm(0.09, 0.4, 2.0, 2.5)\%$ and thus negligible for all conceivable practical applications. The approximation formulae for the $\mathcal{O}(\alpha_s^2 C_F^2)$ and $\mathcal{O}(\alpha_s^2 C_A C_F)$ contributions given in Ref. [8, 20] (using Eqs. (65) and (66) of Ref. [8]) together with the analytically known fermionic corrections agree within 1-2% with our result. We thus confirm the results for the cross section given in Refs. [8, 20].

VIII. ANALYSIS FOR THE VACUUM POLARIZATION AT $\mathcal{O}(\alpha_s^3)$

For the reconstruction of $\Pi^{(3)}$ we use all available information from the expansions in the threshold region, Eqs. (15), the high-energy region, Eqs. (17) and around $z = 0$ in Eqs. (22). For the construction of $\Pi^{(3)}_{\rm reg}$ we account for the first two coefficients in the expansion around $z = 0$, the non-logarithmic term $\propto \sqrt{1-z}$ in the threshold limit and the two constraints from the absence of terms $\sim 1/z^{3/2}$ and $\sim 1/z^{5/2}$ for $|z| \to \infty$. This amounts to 6 constraints on the Padé approximants for method (i), where the Coulomb singularity $\propto 1/(1-z)$ is accounted for in $\Pi^{(3)}_{\rm reg}$, and 5 constraints on the Padé approximants for method (ii), where this Coulomb singularity is accounted for in $\Pi^{(3)}_{\log}$. Thus we have $n+m = 5$ for the Padé approximants $P_{m,n}$ for method (i) and $n+m = 4$ for the Padé approximants $P_{m,n}$ for method (ii).

In Fig. 4 the results for the coefficients $\bar{C}_k^{(30)}$ for $k = 3, 4, 5, 6, 7$, the high-energy constants $H_{0,1}^{(3)}$ and the threshold constant $K^{(3)}$ are displayed for $n_f = n_\ell + 1 = 4$ relevant for charm quark production. The different labels $[m, n]$ which have been added to the upper left panel for $\bar{C}_3^{(30)}$ refer to the Padé approximant used for the respective $\Pi^{(3)}_{\rm reg}$ function and their order is representative for all panels. The error bars represent the range of values covered by the variations of the modification factors as described in Sec. IV, and the blue dashed lines indicate the range covered by all individual results. We adopt this range as the uncertainty in our determination of these coefficients, and the results are summarized together with the corresponding results for $n_f = n_\ell + 1 = 5$ in Tab. IV. For the determination of the high-energy coefficients $H_0^{(3)}$ and $H_1^{(3)}$ we find uncertainties of about 1% and 10%, respectively. This compares well with the corresponding results for $H_0^{(2)}$ and $H_1^{(2)}$ we have obtained at $\mathcal{O}(\alpha_s^2)$ for approximation C, see Fig. 1 and Tab. III. For the coefficients $\bar{C}_k^{(30)}$ with $k \geq 3$ we find somewhat larger relative uncertainties than in for the $\bar{C}_k^{(20)}$ in approximation C. This is, however, not unexpected since the cancellations that arise when the pole mass results for these coefficients are transferred to the $\overline{\rm MS}$ mass scheme are substantially larger at $\mathcal{O}(\alpha_s^3)$. The result for $K^{(3)}$ has

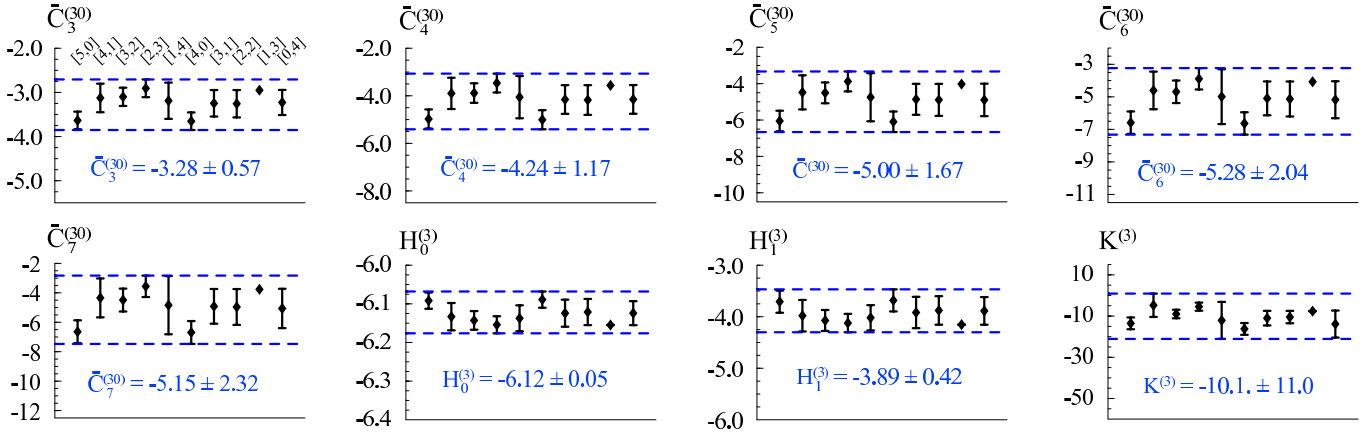

FIG. 4: Results from the reconstructed $\Pi^{(3)}$ function for the coefficients $C^{(30)}_{3,4,5,6,7}$ that arise in the expansion around $z = 0$, for the coefficients $H^{(3)}_{0,1}$ that occur in the non-logarithmic terms in the high-energy expansion $|z| \to \infty$ and for the constant $K^{(3)}$ that appears in the expansion at threshold around $z = 1$. The dashed blue lines represent the envelope of all results obtained from the reconstructed $\Pi^{(3)}$ functions. The individual error bars represent the range of vales obtained from the reconstructed $\Pi^{(3)}$ functions using one particular Padé approximant $P_{m,n}$. The various types of Padé approximants that have been used are indicated in the upper left panel; the same order is used for all other panels. All results are for $n_f = n_\ell + 1 = 4$ running flavors relevant for charm production.

a particularly large error and can merely serve as a rough constraint on its true values. Concerning the precision in the determinations of $K^{(3)}$, we believe that a substantial improvement can be achieved once the full set of NNNLO terms $\propto \sqrt{1-z}$ in the expansion for R at the threshold and the exact values for $\bar{C}_k^{(30)}$ with $k \geq 3$ become available.

	$n_f = 4$	$n_f = 5$
$\bar{C}_1^{(30)}$	-5.6404	-7.7624
$\bar{C}_2^{(30)}$	-3.4937	-2.6438
$\bar{C}_3^{(30)}$	-3.279 ± 0.573	-1.457 ± 0.579
$\bar{C}_4^{(30)}$	-4.238 ± 1.171	-1.935 ± 1.201
$\bar{C}_5^{(30)}$	-4.996 ± 1.666	-2.507 ± 1.732
$\bar{C}_6^{(30)}$	-5.280 ± 2.045	-2.809 ± 2.150
$\bar{C}_7^{(30)}$	-5.151 ± 2.321	-2.847 ± 2.467
$H_0^{(3)}$	-6.122 ± 0.054	-4.989 ± 0.053
$H_1^{(3)}$	-3.885 ± 0.417	-3.180 ± 0.405
$K^{(3)}$	-10.09 ± 11.00	-5.97 ± 10.09

TABLE IV: Summary of the results for the coefficients $C^{(30)}_{3,4,5,6,7}$, $H^{(3)}_{0,1}$ and $K^{(3)}$ obtained from the reconstructed $\Pi^{(3)}$ function for $n_f = n_\ell + 1 = 4$ and $n_f = n_\ell + 1 = 5$. The coefficients $C^{(30)}_{1,2}$ are known exactly and shown for completeness.

One of the most important applications of the coefficients $\bar{C}_n^{(30)}$ is the determination of the $\overline{\text{MS}}$ charm and bottom quark masses from moments M_n of the charm and bottom quark e^+e^- cross section. For small values of n one way to compute the moments is using fixed-order perturbation theory as shown in Eq. (10). Using the results from Tab. IV we find for the fixed-order moments at $\mathcal{O}(\alpha_s^3)$ for charm quarks ($n_f = 4$)

$$\begin{aligned} M_3 &= (0.1348 \pm 0.0044 \pm 0.0005) \times 10^{-2}\,, \\ M_4 &= (0.153 \pm 0.032 \pm 0.002) \times 10^{-3}\,, \\ M_5 &= (0.199 \pm 0.084 \pm 0.008) \times 10^{-4} \\ M_6 &= (0.084 \pm 0.144 \pm 0.036) \times 10^{-5}\,. \end{aligned} \tag{33}$$

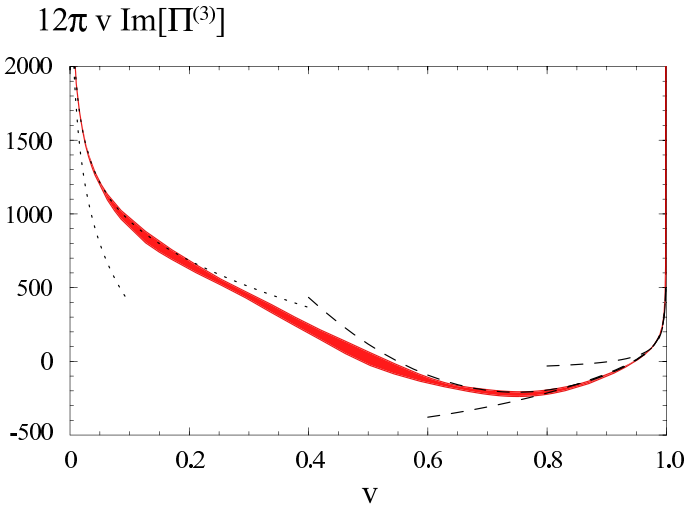

FIG. 5: Result for $12\pi v\mathrm{Im}[\Pi^{(3)}(q^2+i0)]$ as a function of v for $n_f = 4$ using the currently available information for the reconstruction of $\Pi^{(3)}$.The red band represent the uncertainty. The dotted and dashed black lines show the expansions in the threshold and the high-energy region up to next-to-next-to-leading order. See the text for details.

Here we used $\overline{m}_c(\overline{m}_c) = 1.27$ GeV for the $\overline{\rm MS}$ charm mass and $\alpha_s^{(n_f=4)}(1.27\ \text{GeV}) = 0.387637$ for the strong coupling as the input and four-loop renormalization group evolution. The first error arises from the variation of the renormalization scale between 1.27 and 3.81 GeV and the second error is due to the uncertainties in the $\mathcal{O}(\alpha_s^3)$ coefficients $C_k^{(30)}$ shown in Tab. IV. For bottom quarks ($n_f = 5$) with $\overline{m}_b(\overline{m}_b) = 4.17$ GeV and $\alpha_s^{(n_f=5)}(4.17\ \text{GeV}) = 0.224778$ as the input we find

$$\begin{aligned} M_3 &= (2.350 \pm 0.017 \pm 0.002) \times 10^{-7}\,, \\ M_4 &= (2.167 \pm 0.045 \pm 0.005) \times 10^{-9}\,, \\ M_5 &= (2.126 \pm 0.091 \pm 0.011) \times 10^{-11}\,, \\ M_6 &= (2.160 \pm 0.148 \pm 0.022) \times 10^{-13}\,. \end{aligned} \tag{34}$$

The first error arises from the variation of the renormalization scale between 2.085 and 8.34 GeV and the second error is due to uncertainties in the $\mathcal{O}(\alpha_s^3)$ coefficients $C_k^{(30)}$ shown in Tab. IV. The results show that that the uncertainties in $M_{3,4,5}$ caused by the errors in the coefficients $C_{3,4,5}^{(30)}$ we have obtained in this work are an order of magnitude smaller than the overall uncertainties of the moments at $\mathcal{O}(\alpha_s^3)$ due to variations of the renormalization scale. For physically relevant values of n they can be safely neglected.

Finally, let us analyze the $\mathcal{O}(\alpha_s^3)$ corrections to the e^+e^- cross section obtained from the $\Pi^{(3)}$. In Fig. 5 we have plotted the function $12\pi v\mathrm{Im}[\Pi^{(3)}(q^2+i0)]$ for $n_f = 4$ relevant for charm quark production in the pole mass scheme as a function of the quark velocity $v = \sqrt{1-1/z}$. As for the analysis in Fig. 3 we have included the factor v to suppress the Coulomb singularity. The function still diverges logarithmically for $v \to 0$ because the $\mathcal{O}(\alpha_s^3)$ cross section has a singularity $\sim \ln(v)/v$ in the nonrelativistic limit. The red shaded band is the area covered by all solutions for $\Pi^{(3)}$ that pass the criteria discussed in Sec. VI and represents the uncertainty. The relative uncertainty is about 10% at $v = 0.2$ and 0.8 and should be acceptable for most applications where $\mathcal{O}(\alpha_s^3)$ accuracy is required. For comparison we have also displayed the expansions in the threshold region for $v \to 0$ (dotted lines) at NLO (short line) and at NNLO (long line). Likewise the expansions in the high-energy limit for $v \to 1$ (dashed lines) are shown, where the short line refers to order $1/z^0$, the medium-length line to order $1/z$ and the longest lines to order $1/z^2$. We strongly emphasize the importance of incorporating the NNLO contributions in the expansion close to the threshold and the $1/z^2$ terms at high energies for achieving our result. Once more information from the different kinematic regions becomes available, the uncertainties can be further reduced substantially.

IX. CONCLUSIONS

In this work we have determined the full mass and q^2 dependence of the $\mathcal{O}(\alpha_s^2)$ and $\mathcal{O}(\alpha_s^3)$ corrections to the heavy quark vacuum polarization function $\Pi(q^2, m^2)$ and its contribution to the e^+e^- total cross section. Our approach uses known results for the expansions of $\Pi(q^2, m^2)$ at high energies, in the threshold region and around $q^2 = 0$, conformal mapping and the Padé approximation method. We have demonstrated for the vacuum polarization function at $\mathcal{O}(\alpha_s^2)$ that the approach allows for reliable determinations of other properties of Π with small uncertainties, and that the uncertainties of the results can be systematically reduced if more information from the three different kinematic regions is accounted for. Our results for the cross section at $\mathcal{O}(\alpha_s^2)$ also confirm previous results by Chetyrkin, Kühn and Steinhauser from Refs. [8, 20]. For the vacuum polarization function at $\mathcal{O}(\alpha_s^2)$ we have determined the previously unknown non-logarithmic constant term that arises at NLO in the expansion close to the threshold. For the $\mathcal{O}(\alpha_s^3)$ corrections to the vacuum polarization function we determined the previously unknown coefficients in the expansion around $q^2 = 0$ beyond order q^4 and the first two non-logarithmic coefficients in the high-energy expansion. The results for the coefficients in the expansion around $q^2 = 0$ allow for the determination of the moments M_n of the e^+e^- cross section for $n \geq 3$ at $\mathcal{O}(\alpha_s^3)$.

X. ACKNOWLEDGEMENTS

We thank K. Chetyrkin, H. Kühn and M. Steinhauser for useful converstion and comments to the manuscript. M. Zebarjad thanks the MPI for hospitality while this work was accomplished and the MPI guest program for partial support. This work was supported in part by the EU network contract MRTN-CT-2006-035482 (FLAVIAnet).

Note added: After completion of this work K. Chetyrkin pointed out to us that analytic expressions for the constants $H_1^{(3)}$ can be derived from results given in Ref. [32]. Evaluated numerically they give $H_1^{(3)} = -4.33306$ for $n_f = 4$ and $H_1^{(3)} = -3.53165$ for $n_f = 5$ which is in agreement with the results we have presented in Tab. IV.

[1] V. A. Novikov et al., Phys. Rept. **41**, 1 (1978).
[2] L. J. Reinders, H. Rubinstein, and S. Yazaki, Phys. Rept. **127**, 1 (1985).
[3] A. O. G. Kallen and A. Sabry, Kong. Dan. Vid. Sel. Mat. Fys. Med. **29N17**, 1 (1955).
[4] B. A. Kniehl, Phys. Lett. **B237**, 127 (1990).
[5] A. H. Hoang, M. Jezabek, J. H. Kuhn, and T. Teubner, Phys. Lett. **B338**, 330 (1994), hep-ph/9407338.
[6] A. H. Hoang, J. H. Kuhn, and T. Teubner, Nucl. Phys. **B452**, 173 (1995), hep-ph/9505262.
[7] K. G. Chetyrkin, J. H. Kuhn, and M. Steinhauser, Phys. Lett. **B371**, 93 (1996), hep-ph/9511430.
[8] K. G. Chetyrkin, J. H. Kuhn, and M. Steinhauser, Nucl. Phys. **B482**, 213 (1996), hep-ph/9606230.
[9] M. Czakon and T. Schutzmeier, JHEP **07**, 001 (2008), 0712.2762.
[10] K. G. Chetyrkin, R. V. Harlander, and J. H. Kuhn, Nucl. Phys. **B586**, 56 (2000), hep-ph/0005139.
[11] R. V. Harlander and M. Steinhauser, Comput. Phys. Commun. **153**, 244 (2003), hep-ph/0212294.
[12] A. H. Hoang and T. Teubner, Phys. Rev. **D58**, 114023 (1998), hep-ph/9801397.
[13] A. H. Hoang, Phys. Rev. **D56**, 7276 (1997), hep-ph/9703404.
[14] K. G. Chetyrkin, J. H. Kuhn, and C. Sturm, Eur. Phys. J. **C48**, 107 (2006), hep-ph/0604234.
[15] R. Boughezal, M. Czakon, and T. Schutzmeier, Phys. Rev. **D74**, 074006 (2006), hep-ph/0605023.
[16] A. Maier, P. Maierhofer, and P. Marqaurd (2008), 0806.3405.
[17] J. Fleischer and O. V. Tarasov, Z. Phys. **C64**, 413 (1994), hep-ph/9403230.
[18] D. J. Broadhurst, J. Fleischer, and O. V. Tarasov, Z. Phys. **C60**, 287 (1993), hep-ph/9304303.
[19] P. A. Baikov and D. J. Broadhurst (1995), hep-ph/9504398.
[20] K. G. Chetyrkin, J. H. Kuhn, and M. Steinhauser, Nucl. Phys. **B505**, 40 (1997), hep-ph/9705254.
[21] A. H. Hoang and M. Jamin, Phys. Lett. **B594**, 127 (2004), hep-ph/0403083.
[22] J. H. Kuhn, M. Steinhauser, and C. Sturm, Nucl. Phys. **B778**, 192 (2007), hep-ph/0702103.
[23] A. H. Hoang, Phys. Rev. **D59**, 014039 (1999), hep-ph/9803454.
[24] A. H. Hoang, Phys. Rev. **D61**, 034005 (2000), hep-ph/9905550.
[25] A. Czarnecki and K. Melnikov, Phys. Rev. lett. **80**, 2531 (1998), hep-ph/9712222.
[26] A. H. Hoang, A. V. Manohar, I. W. Stewart, and T. Teubner, Phys. Rev. **D65**, 014014 (2002), hep-ph/0107144.
[27] A. H. Hoang et al., Eur. Phys. J. direct **C2**, 1 (2000), hep-ph/0001286.
[28] K. G. Chetyrkin and J. H. Kuhn, Nucl. Phys. **B432**, 337 (1994), hep-ph/9406299.
[29] K. G. Chetyrkin, R. Harlander, J. H. Kuhn, and M. Steinhauser, Nucl. Phys. **B503**, 339 (1997), hep-ph/9704222.

[30] A. Maier, P. Maierhofer, and P. Marquard, Nucl. Phys. **B797**, 218 (2008), 0711.2636.
[31] R. Boughezal, M. Czakon, and T. Schutzmeier, Nucl. Phys. Proc. Suppl. **160**, 160 (2006), hep-ph/0607141.
[32] P. A. Baikov, K. G. Chetyrkin, and J. H. Kuhn, Nucl. Phys. Proc. Suppl. **135**, 243 (2004).